Optical Properties of Single-Crystal Paratellurite (TeO_2)

Naoya Uchida
Musashino Electrical Communication Laboratory,
Nippon Telegraph and Telephone Public Corporation, Musashino, Tokyo, Japan
(Received 7 January 1971)

Absorption at the fundamental band edge, the dispersion characteristics of the refractive indices, the optical rotatory power, associated temperature coefficients, and the photoelastic constants have been investigated. Absorption at the band edge has been found to obey the exponential Urbach rule up to $5\times10^2\,\mathrm{cm}^{-1}$. Refractive-index data between 0.4 and 1.0 μm are excellently fitted to the two-term Sellmeier dispersion formula with oscillators located at 9.24 and 4.70 eV. The contribution of the former oscillator to the refractive index in the visible to infrared region is larger than that of the latter. The dispersion energy $\mathcal{E}_{di}=\mathcal{F}_i/\mathcal{E}_i$ (where $\mathcal{F}_i$ is the oscillator strength factor and $\mathcal{E}_i$ is the oscillator position) defined by Wemple and DiDomenico has been determined as ~ 25 eV for the transition at 9.24 eV, and is in agreement with the value derived for the average single oscillator. Dispersion of the rotatory power has been also explained by the two-term Chandrasekhar's formula with oscillator positions nearly equal to those found from the refractive indices. Dispersion measurements of the photoelastic constants reveal that a large anisotropy exists between the changes of $\mathcal{F}_i$ and $\mathcal{E}_i$ induced by the strain S_1 and those induced by S_3. The main contribution to the positive value of the temperature coefficient of the refractive indices comes from an intrinsic temperature effect, and the contribution of the photoelastic effect associated with the thermal expansion is negative. Anomalous behavior has been observed in $dn/n\,dT$ and $d\rho/\rho\,dT$ between 0.5 and 0.6 μm, and is probably attributable to extremely weak absorption peaks located in this wavelength region.

I. INTRODUCTION

Paratellurite single crystals were first grown by Liebertz[1] using the Czochralski method, and some interesting features in its acoustic, piezoelectric, and optical properties were reported.[1,2] Elasto-optical properties of the crystal were reported by this author,[3] and a few sound modes were found to be useful for acousto-optical device applications. This crystal belongs to point group D_4 (422), and the structure is distorted rutile type composed of considerably deformed TeO_6 octahedra.[4]

Recently, Wemple and DiDemenico[5,6] investigated dispersion characteristics of the refractive index in widely different nonmetallic compounds, and proposed a simple and unified approach for the explanation of the dispersion behavior using the dispersion energy concept. Although the behavior in TeO_2 is also included in this approximate unification,[6] detailed investigations of the optical properties of this crystal with its unique structure are interesting and will be useful for the development of the dispersion energy concept.

This paper describes the dispersion characteristics of the refractive indices, birefringence, optical rotatory power along the optic axis, photoelastic constants, and temperature coefficients of the refractive indices and the rotatory power mainly in the visible spectral region. Absorption data at the fundamental band edge in the ultraviolet region are also given.

Some phenomenological analyses of the dispersion of the refractive indices and rotatory power are made using the well-known Sellmeier dispersion formula and Chandrasekhar's formula,[7] respectively. Although the analyses basically follow the treatments made by Wemple and DiDomenico,[5,6] we here emphasize the importance of a two-oscillator model instead of their average single-oscillator model. Two-oscillator parameters obtained from the experimental data are discussed and compared with the single-oscillator parameters. Thermo-optic behavior[8] of this crystal is also discussed in relation to the dispersion characteristics of the photoelastic constants.[9,10]

II. EXPERIMENTAL PROCEDURES

Absorption spectra were measured with a spectrophotometer for wavelengths between 0.3 and 0.7 μm. Three kinds of specimens were prepared. One was a cubic solid about $10\times10\times10$ mm in size oriented along the principal axes. The other specimens were two (100) plates 109 and 15 μm thick.

Indices of refraction were measured with a spectrometer by the method of minimum deviation in the wavelength region between 0.4 and 1.0 μm. A prism was used in which a plane $(hk0)$ makes an acute angle of approximately 29° with a plane $(h\bar{k}0)$ with (100) as a prism bisectrix plane.

Measurements of the rotatory power along the c axis were made with the cube-shaped specimen described above. The approximate values of the

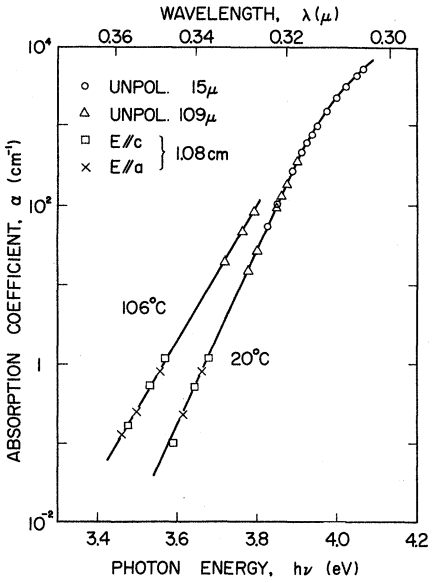

FIG. 1. Spectral dependence of the optical absorption coefficient in TeO_2 at 20 and 106 °C.

rotatory power had previously been determined using thin plate specimens.[11] The linearly polarized light beam was chopped at 1 kHz, and the extinction position of an analyzer placed behind the specimen was detected by a tuned amplifier.

Dispersion characteristics of the photoelastic constants were measured by the ultrasonic-light-diffraction technique for two kinds of rectangular solid specimens; one was oriented along the principal axes and the other was oriented along the c axis and the [110] directions. Pulsed ultrasonic waves of 50–150 MHz were launched into the crystal by $LiNbO_3$ transducers. Signs of the photoelastic constants were determined using a Mach-Zehnder interferometer by observing the shift of the interference fringes under a uniaxial compressive stress.

All specimens were oriented to better than ± 0.5°.

III. EXPERIMENTAL RESULTS

The absorption data at the fundamental absorption edge for three different specimens are shown in Fig. 1 as a function of photon energy $h\nu$. Polarized light was used for the thickest specimen, and unpolarized light was used for the other two specimens. Difference between the absorption behavior for $E \parallel a$ axis and $E \parallel c$ axis is very small. The data obey an exponential Urbach tail[12] of the following form, until α reaches 5×10^2 cm^{-1}:

$$\alpha = \alpha_0 e^{(h\nu - \mathcal{E}_0)/\eta kT}, \qquad (1)$$

where $\mathcal{E}_0$ is related to the band gap energy, k is Boltzmann's constant, and T is the absolute temperature.[13] The value of η is found to be approximately constant over the present temperature range: 1.49 at 20 °C and 1.53 at 106 °C. These values are comparable to those of perovskite-type dielectric materials.[13,14] The shift of the band edge was linear with temperature between 20 and 106 °C with temperature coefficients $d\mathcal{E}/\mathcal{E}\,dT$ having values of -3.5×10^{-4} and -1.5×10^{-4}/°C at $\alpha = 1$ and 10^2 cm^{-1}, respectively.

Figure 2 shows dispersion characteristics of the indices of refraction at 20 °C in the wavelength region between 0.4 and 1.0 μm. Selected values are listed in Table I with the maximum error estimated from the experimental accuracy and the limit of sample misorientation. The values at 0.5893 μm have been previously reported by Liebertz,[1] and the present results are in excellent agreement with his data.

Dispersion of the optical rotatory power along the optic axis is shown in Fig. 3. The sense of the rotation observed in the present specimens was always left handed, and the negative sign is assigned by the usual definition.[15] Selected values are listed in Table II along with the estimated accuracy. The value at 0.5893 μm is in good agreement with published data.[2,11]

The temperature dependence of the refractive indices was measured from room temperature to 130 °C in the wavelength region between 0.415 and 0.67 μm. The temperature coefficient $dn/n\,dT$ at 25 °C is plotted in Fig. 4 as a function of wavelength. Anomalous behavior is observed between 0.47 and 0.6 μm for both ordinary and extraordi-

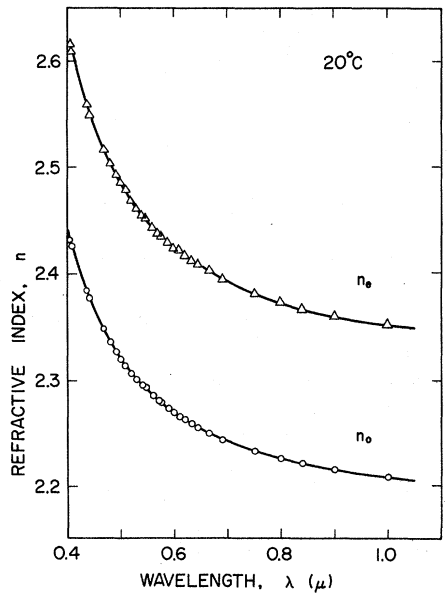

FIG. 2. Dispersion of the refractive indices n_o and n_e in TeO_2 at 20 °C. The full curves are calculated with Eq. (4) using the two-oscillator parameters listed in Table III.

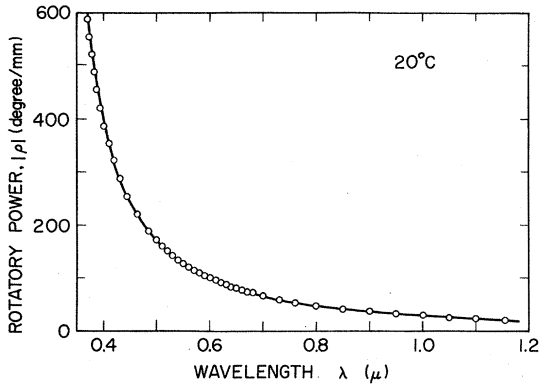

FIG. 3. Dispersion of the optical rotatory power along the optic axis in TeO_2 measured at 20 °C. The full curve is calculated with Eq. (7) using the two-oscillator parameters listed in Table III.

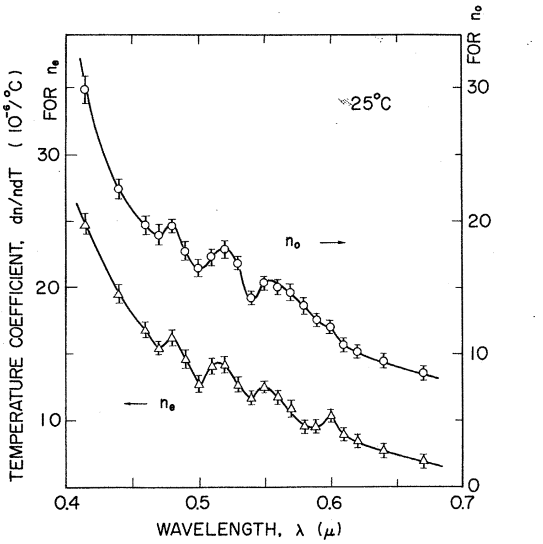

FIG. 4. Dispersion of the temperature coefficients of the refractive indices in TeO_2 at 25 °C.

nary indices. The anomaly diminishes somewhat at temperatures above 50–60 °C. However, the present experimental accuracy was insufficient to distinguish the difference clearly.

The temperature dependence of the optical rotatory power was measured from room temperature to 120 °C between 0.405 and 0.8 μm. The coefficient $d\rho/\rho\, dT$ is shown in Fig. 5 as a function of wavelength at 25 and 80 °C. An anomalous dispersion behavior is also observed between 0.5 and 0.6 μm. The slope of the ρ-vs-T curve gradually changed its value in the vicinity of 50 °C in this wavelength region, while it was unchanged outside this region. As can be seen from the insert in this figure, the anomaly observed at 25 °C is somewhat larger than that at 80 °C.

It is known that the relative signs of the photoelastic constants p_{12}, p_{13}, p_{31}, and p_{33} are the same, and are opposite to those of p_{44} and p_{66}, from measurements of the acousto-optical figure of merit for several oblique-cut specimens.[3] The sign of p_{11} could not be determined because of its extremely small value. An attempt was made to determine the absolute signs of the piezo-optic constants $\pi_{ik} = p_{ij}s_{jk}$ (where s_{jk} is the elastic compliance coefficient) and, consequently, those of the photoelastic constants by the interferometric method. The specimen was laid in one of the optical path arms of the Mach-Zehnder interferometer, and the shift of the interference fringes was observed under unidirectional compressive stress T_k. The change of retardation $\Delta\Gamma_i$ per unit length along the a axis induced by the stress T_3, for instance, is given by

TABLE I. Selected values of the refractive indices in TeO_2 at 20 °C. Calculated values for the single- and the two-oscillator models are also given for comparison. Parameters used for the calculation are listed in Table III.

Wavelength λ (μm)	n_o Observed	n_o Calculated Single-osc. model	n_o Calculated Two-osc. model	n_e Observed	n_e Calculated Single-osc. model	n_e Calculated Two-osc. model
0.4047	2.4315 ± 0.0009	2.4190	2.4318	2.6157 ± 0.0010	2.6045	2.6159
0.4358	2.3834 ± 0.0007	2.3781	2.3832	2.5583 ± 0.0008	2.5544	2.5583
0.4678	2.3478 ± 0.0007	2.3462	2.3476	2.5164 ± 0.0008	2.5155	2.5163
0.4800	2.3366 ± 0.0006	2.3360	2.3366	2.5036 ± 0.0008	2.5032	2.5033
0.5086	2.3150 ± 0.0006	2.3155	2.3150	2.4779 ± 0.0007	2.4783	2.4778
0.5461	2.2931 ± 0.0006	2.2941	2.2931	2.4520 ± 0.0007	2.4525	2.4520
0.5893	2.2738 ± 0.0006	2.2750	2.2740	2.4295 ± 0.0007	2.4295	2.4297
0.6328	2.2597 ± 0.0006	2.2601	2.2594	2.4119 ± 0.0007	2.4116	2.4119
0.6438	2.2562 ± 0.0006	2.2568	2.2563	2.4086 ± 0.0007	2.4077	2.4088
0.690	2.2450 ± 0.0006	2.2450	2.2449	2.3955 ± 0.0007	2.3935	2.3955
0.800	2.226 ± 0.0015	2.2251	2.2262	2.373 ± 0.0015	2.3697	2.3735
1.00	2.208 ± 0.0015	2.2051	2.2077	2.352 ± 0.0015	2.3459	2.3519

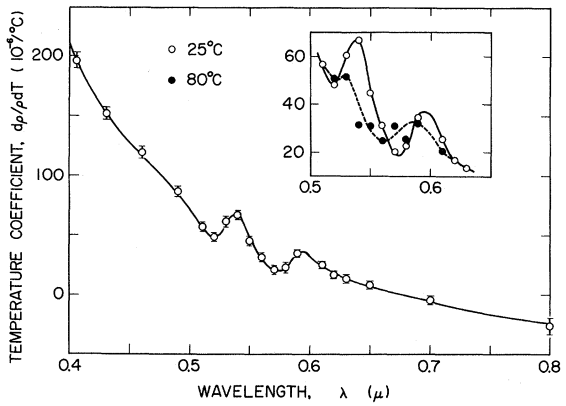

FIG. 5. Dispersion of the temperature coefficient of the rotatory power in TeO_2 at 25 and 80 °C.

$$\Delta\Gamma_i \equiv \Delta\gamma_i T_3 = (-\tfrac{1}{2}n_i^3\pi_{i3} + n_i s_{13})T_3 \,, \tag{2}$$

where the subscript i takes 1 or 3 corresponding to the ordinary or extraordinary ray, respectively. Using the published data on p_{ij}[3] and s_{jk},[16] we can write

$$\Delta\gamma_1 = (\mp 1.9 - 0.5)\times 10^{-11}\ \mathrm{m^2/N}\,,$$

and

$$\Delta\gamma_3 = (\mp 1.6 - 0.5)\times 10^{-11}\ \mathrm{m^2/N}\,. \tag{3}$$

The minus sign corresponds to positive values of p_{12}, p_{13}, etc., and the plus sign corresponds to negative values of these components. The contribution of $-\frac{1}{2}n_i^3\pi_{i3}$ to $\Delta\gamma_i$ is dominant within the tolerance of the experimental accuracy in p_{ij} and s_{jk}, and thus a unique and definite determination of the signs is possible. Retardations $\Delta\Gamma_1$ and $\Delta\Gamma_3$ were observed to increase under the compressive stress T_3 usually defined as being negative.[17] Therefore, $\Delta\gamma_1$ and $\Delta\gamma_3$ were negative, and the photoelastic constants p_{12}, p_{13}, p_{31}, and p_{33} are determined to be positive.

Figure 6 shows the dispersion of the photoelastic constants at room temperature measured by the ultrasonic light diffraction technique. The dispersion of p_{13} and p_{33} is strongly negative and that of p_{31} is weakly negative. On the other hand, slightly positive dispersion is observed for $p_{12}-p_{11}$.

IV. DISCUSSION

It is well known that the refractive index of nonmetallic materials in the region of low absorption is given by the Sellmeier dispersion formula

$$n_i^2 - 1 = \sum_s \mathcal{F}_i^{(s)}/(\mathcal{E}_i^{(s)2} - \mathcal{E}^2)\,, \tag{4}$$

where $\mathcal{F}_i^{(s)} = h^2 N_i^{(s)} f_i^{(s)}/\pi m$, $\mathcal{E}_i^{(s)} = hc/e\lambda_i^{(s)}$, and $\mathcal{E} = hc/e\lambda$. The symbol $N_i^{(s)}$ is the number of oscillator per unit volume, $f_i^{(s)}$ is the oscillator strength or transition probability, $\lambda_i^{(s)}$ is the oscillator position, h is Planck's constant, c is the velocity of light, and e and m are the electronic charge and mass, respectively. DiDomenico and Wemple[5,6] recently investigated the dispersion behavior of widely different materials including oxides, halides, and II-VI and III-V semiconductors. They showed that the refractive index is well explained by the single-oscillator model

TABLE II. Selected values of the optical rotatory power along the optic axis in TeO_2 at 20 °C. Calculated values for the single- and the two-oscillator models are also listed here. Parameters used for the calculation are given in Table III.

Wavelength	|ρ| (deg/mm)		
		Calculated	
λ (μm)	Observed	Single-osc. model	Two-osc. model
0.3698	587.1±1.9	532.2	589.0
0.3783	520.6±1.8	479.4	521.0
0.3917	437.4±1.5	411.9	437.6
0.4152	337.6±1.5	325.4	336.8
0.4382	271.0±1.1	266.0	271.1
0.4630	221.1±1.2	219.6	221.4
0.4995	171.2±0.9	171.6	171.6
0.530	143.4±0.9	143.2	142.7
0.5893	104.9±0.5	105.8	105.2
0.6328	86.9±0.5	87.3	86.8
0.700	67.4±0.6	67.4	67.1
0.800	48.5±0.6	48.7	48.5
0.900	37.4±0.6	37.0	37.0
1.00	29.5±0.6	29.2	29.3
1.10	23.8±0.6	23.6	23.7

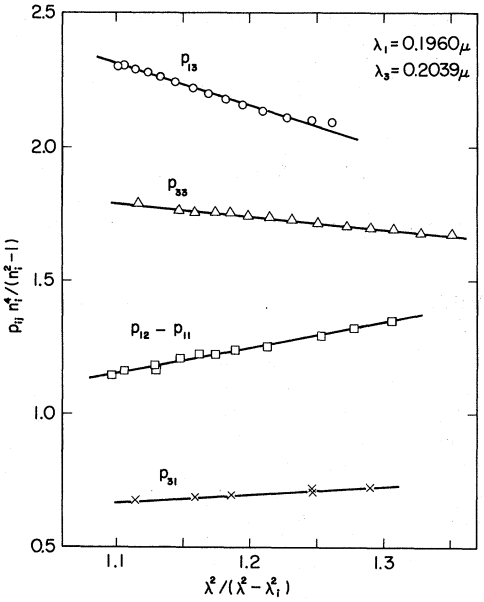

FIG. 6. Dispersion of the photoelastic constants in TeO_2 at room temperature.

$$n_i^2 - 1 = \mathcal{F}_i/(\mathcal{E}_i^2 - \mathcal{E}^2)\,, \tag{5}$$

where $\mathcal{F}_i$ means an average oscillator strength factor and $\mathcal{E}_i$ is an average oscillator position. They also arrived at the remarkable result that the dispersion energy $\mathcal{E}_{di}$, defined by

$$\mathcal{E}_{di} = \mathcal{F}_i/\mathcal{E}_i\,, \tag{6}$$

is essentially the same among all ionic compounds and, similarly, among all covalent ones when normalized by the product of the cation coordination number N_c, anion valency Z_a, and number of effective valence electrons per anion N_e.[6] In other words, $\mathcal{E}_{di}$ itself is the same, for instance, in all ionic oxides ($Z_a = 2$) with the same cation coordination number and effective valence electron number. The value of $\mathcal{E}_{di}$ was experimentally given as ~25 eV for oxygen-octahedra dielectrics.[6]

Plotting $1/(n_i^2 - 1)$ vs $1/\lambda^2$ for TeO_2 using the data shown in Fig. 2 gave a linear relation in the middle wavelength region 0.45–0.75 μ m, but systematic and significant deviation from the linear relation was observed outside this region. Similar behavior, especially at the shorter wavelengths, is also observed in several other materials such as TiO_2,[18,19] $SrTiO_3$[18,20,21] (published data on these crystals are graphically examined by the present author), $BaTiO_3$,[22] and Pb_2MoO_5.[23] This feature exhibits the limitation of the validity of the averaged single-oscillator dispersion relation. Thus, in the present treatment, an attempt is made to explain the data by a two-oscillator model, and the parameters $\mathcal{F}_i^{(s)}$ and $\mathcal{E}_i^{(s)}$ in Eq. (4), calculated with the least-squares method, are listed in Table III. Single-term parameters fitted to the data in the middle wavelength region are also listed in this table. Calculated values of the refractive indices using these parameters are given in Table I. The two-oscillator fit is excellent over the entire wavelength range (the results are also shown in Fig. 2 by the full curves), while the single-oscillator fit is restricted within the middle wavelength region.

Dispersion energies $\mathcal{E}_{di}$ with respect to the single-oscillator model are evaluated as 23.5 and 26.2 eV for the ordinary and extraordinary rays, respectively.[24] The crystal structure of TeO_2 is distorted rutile type, in which each Te atom is surrounded by six oxygens: two oxygens at a distance of 1.91 Å, two at 2.09 Å, and two at 2.89 Å.[4] If we consider that the cation coordination number N_c is 6, this crystal is classified as ionic similarly to the BO_6-type dielectric and ferroelectric materials. However, there is no indisputable evidence to support the above consideration and the crystal still has another possibility to be (more or less) covalent corresponding to the "effective" N_c between 4 and 6.

The two-oscillator parameters listed in Table

TABLE III. Fitted values of the single- and the two-oscillator parameters for TeO_2 at 20 °C. Definitions of the symbols are given in Eqs. (4)–(9).

	Single-oscillator model					Two-oscillator model								
	$\mathcal{F}_i$ (eV²)	λ_i (μm)	$\mathcal{E}_i$ (eV)	$\mathcal{E}_{di}$ (eV)	S_{1i} (rad eV² μm⁻¹)	$\mathcal{F}_i^{(1)}$ (eV²)	$\lambda_i^{(1)}$ (μm)	$\mathcal{E}_i^{(1)}$ (eV)	$\mathcal{E}_{di}^{(1)}$ (eV)	$S_1^{(1)}$ (rad eV² μm⁻¹)	$\mathcal{F}_i^{(2)}$ (eV²)	$\lambda_i^{(2)}$ (μm)	$\mathcal{E}_i^{(2)}$ (eV)	$\mathcal{E}_{di}^{(2)}$ (eV)
n_o	148.6	0.1960	6.33	23.5	0.2309	220.6	0.1342	9.24	23.9	0.8838	25.55	0.2638	4.70	5.44
n_e	159.6	0.2039	6.08	26.2	0.2345	241.0	0.1342	9.24	26.1	0.8754	34.20	0.2631	4.71	7.26
	S_{1i} (rad eV² μm⁻¹)	λ_i' (μm)	$\mathcal{E}_i'$ (eV)	$\mathcal{E}_{di}'$ (meV)		$S_1^{(1)}$ (rad eV² μm⁻¹)	$\lambda_1^{(1)}$ (μm)	$\mathcal{E}_1^{(1)}$ (eV)	$\mathcal{E}_{d1}'^{(1)}$ (meV)		$S_1^{(2)}$ (rad eV² μm⁻¹)	$\lambda_1^{(2)}$ (μm)	$\mathcal{E}_1^{(2)}$ (eV)	$\mathcal{E}_{d1}'^{(2)}$ (meV)
$\lvert\rho\rvert$	0.2309	0.2345	5.29	10.2		0.8838	0.1331	9.31	12.6		0.08754	0.2645	4.69	3.98

TABLE IV. Fitted values of the single- and the two-oscillator parameters for TiO_2, $SrTiO_3$, and $LiNbO_3$.

		Single-oscillator model			Two-oscillator model						
		$\mathcal{F}_i$ (eV^2)	$\mathcal{E}_i$ (eV)	$\mathcal{E}_{di}$ (eV)	$\mathcal{F}_i^{(1)}$ (eV^2)	$\mathcal{E}_i^{(1)}$ (eV)	$\mathcal{E}_{di}^{(1)}$ (eV)	$\mathcal{F}_i^{(2)}$ (eV^2)	$\mathcal{E}_i^{(2)}$ (eV)	$\mathcal{E}_{di}^{(2)}$ (eV)	R_i
TiO_2	n_o	126	5.11	24.7	195	8.5	22.9	38.8	4.19	9.3	1.2
	n_e	150	4.95	30.3	226	8.5	26.6	52.2	4.13	12.6	1.0
$SrTiO_3$		137	5.75	23.9	245	9.5	25.7	27.2	4.3	6.3	1.8
$LiNbO_3$	n_o	175	6.72	26.1	215	9.5	22.6	42.4	5.3	8.0	1.6
	n_e	177	7.07	25.1	215	9.5	22.6	33.7	5.36	6.3	2.0

III exhibit some interesting features. First, the oscillator positions for n_o are nearly equal to those for n_e. This feature may correspond to the small dichroism observed at the fundamental band edge, as shown in Fig. 1. Second, it can be seen that the oscillator strength factor $\mathcal{F}_i^{(1)}$ is much larger than $\mathcal{F}_i^{(2)}$, and $\mathcal{F}_i^{(1)}/(\mathcal{E}_i^{(1)})^2$ is still larger than $\mathcal{F}_i^{(2)}/(\mathcal{E}_i^{(2)})^2$. The factor $R_i = \mathcal{F}_i^{(1)}(\mathcal{E}_i^{(2)})^2/\mathcal{F}_i^{(2)}(\mathcal{E}_i^{(1)})^2$ defined by DiDomenico and Wemple[5] is, therefore, larger than unity, 2.2 for n_o and 1.8 for n_e. This feature indicates that the contribution of oscillator (1) located at 9.24 eV to the refractive index is larger than that of oscillator (2) at 4.7 eV at the low-energy region ($\mathcal{E} \to 0$). This trend is also valid in the visible region, although the latter contribution increases as $\mathcal{E}$ becomes large. It should also be noted that dispersion energies $\mathcal{E}_{d1}^{(1)}$ and $\mathcal{E}_{d3}^{(1)}$ are in excellent agreement, respectively, with $\mathcal{E}_{d1}$ and $\mathcal{E}_{d3}$ defined for the single-oscillator model. The latter two features are also verified for TiO_2, $SrTiO_3$, $BaTiO_3$, and other BO_6-type oxides by the application of the two-oscillator model to the dispersion data of these materials. A few results of the calculation are summarized in Table IV for TiO_2,[18,19] $SrTiO_3$,[18,20,21] and $LiNbO_3$.[25] Oscillator positions $\mathcal{E}_i^{(1)}$ and $\mathcal{E}_i^{(2)}$ of these materials roughly coincide with those of two main reflection peaks,[26,27] i.e., C and A peaks designated by Cardona.[26] The dispersion energy $\mathcal{E}_{di}^{(1)}$ is not so different from $\mathcal{E}_{di}$ and the factor R is generally larger than unity in these materials, too. It may be considered that some analogy in the optical properties exists between TeO_2 and BO_6-type oxides, but further experimental evidence is necessary for confirmation of this relation.

Chandrasekhar[7] investigated the dispersion of the optical rotatory power in quartz, benzil, cinnabar, etc., and proposed a dispersion formula considering the feasibly coupled oscillators with resonant frequencies slightly different from each other. The rotatory power along the optic axis is represented by the following formula in the low-absorption region:

$$\rho = \sum_s \mathcal{G}_1^{(s)} \mathcal{E}^2/(\mathcal{E}_1^{(s)2} - \mathcal{E}^2)^2 , \tag{7}$$

where $\mathcal{G}_1^{(s)} = \pi^2 g_1^{(s)} \mathcal{F}_1^{(s)}$, and $g_1^{(s)}$ indicates the gyration factor, including the splitting of the frequencies. When the single-oscillator model is used, Eq. (7) yields

$$\rho = \mathcal{G}_1 \mathcal{E}^2/(\mathcal{E}_1'^2 - \mathcal{E}^2)^2 , \tag{8}$$

where $\mathcal{E}_1' (= hc/e\lambda_1')$ means the average oscillator position with respect to the rotatory power.

Plotting of $1/\lambda\rho^{1/2}$ vs $1/\lambda^2$ for TeO_2 according to Eq. (8) showed an approximately linear relation similar to that observed in the dispersion of the refractive indices. Parameters of the single-oscillator model obtained by this plot are listed in Table III, and the calculated values of ρ are shown in Table II. The parameters for the two-oscillator model obtained by a least-squares method are listed in Table III, and the calculated values of ρ are given in Table II. Observed values excellently fit those calculated from the two-oscillator parameters, while the disagreement in the short-wavelength region is serious in the case of the single-oscillator model. Two oscillator positions $\mathcal{E}_1^{(1)}$ and $\mathcal{E}_1^{(2)}$ are in good agreement with those derived from the refractive index data. The strength factor $\mathcal{G}_1^{(1)}$ is ten times larger than $\mathcal{G}_1^{(2)}$, and the feature mainly comes from the difference between $\mathcal{F}_1^{(1)}$ and $\mathcal{F}_1^{(2)}$ [see Eq. (7)]. A dispersion energy $\mathcal{E}_{d1}'^{(s)}$ may be defined by

$$\mathcal{E}_{d1}'^{(s)} = (hc/e)\mathcal{G}_1^{(s)}/\mathcal{E}_1^{(s)2} , \tag{9}$$

in analogy with that of the refractive index. Calculated values of $\mathcal{E}_{d1}'^{(s)}$ are given in Table III, and it is noted that $\mathcal{E}_{d1}'^{(1)}$ for the oscillator located at 9.31 eV is nearly equal to $\mathcal{E}_{d1}'$ for the averaged oscillator at 5.29 eV.

A dispersion relation for the birefringence $\Delta n\ (= n_e - n_o)$ in the low-absorption region as derived from Eq. (4) is

$$\Delta n (n_e + n_o) = \sum_s (n_o^2 - 1)^{(s)}$$

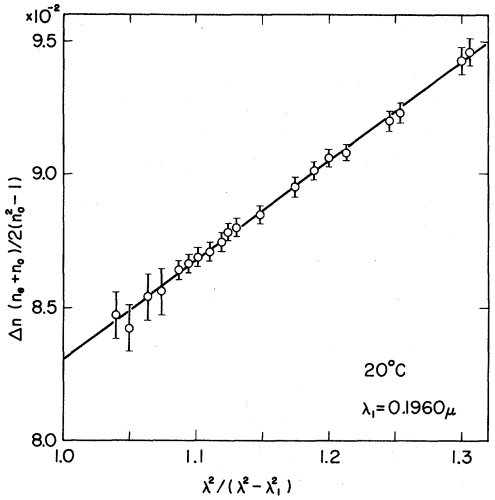

FIG. 7. Dispersion of the birefringence in TeO_2 at 20 °C plotted using Eq. (11) for the single-oscillator model.

$$\times\left[-\frac{\mathcal{E}_1^{(s)2}}{\mathcal{E}_1^{(s)2}-\mathcal{E}^2}\,2\left(\frac{\Delta\mathcal{E}^{(s)}}{\mathcal{E}_1^{(s)}}\right)+\left(\frac{\Delta\mathcal{F}^{(s)}}{\mathcal{F}_1^{(s)}}\right)\right], \quad (10)$$

where $\Delta\mathcal{E}^{(s)}=\mathcal{E}_3^{(s)}-\mathcal{E}_1^{(s)}$ and $\Delta\mathcal{F}^{(s)}=\mathcal{F}_3^{(s)}-\mathcal{F}_1^{(s)}$, assuming that $\Delta\mathcal{E}^{(s)}$ and $\Delta\mathcal{F}^{(s)}$ are small. As shown above, the two-oscillator model is naturally preferable to discuss the dispersion behavior of Δn. However, considering the rather poor accuracy in the birefringence data compared with those of n_i and ρ, further discussion will be based on the single-oscillator model. (The situation is the same in the cases of $dn/n\,dT$, $d\rho/\rho\,dT$, and p_{ij}, which will be discussed later.) This model yields the relation

$$\frac{\Delta n\,(n_e+n_o)}{2(n_o^2-1)}=-\frac{\lambda^2}{\lambda^2-\lambda_1^2}\left(\frac{\Delta\mathcal{E}}{\mathcal{E}_1}\right)+\frac{1}{2}\left(\frac{\Delta\mathcal{F}}{\mathcal{F}_1}\right), \quad (11)$$

which is essentially the same as that given by DiDomenico and Wemple.[5] The relation between $\Delta n\,(n_e+n_o)/2(n_o^2-1)$ and $\lambda^2/(\lambda^2-\lambda_1^2)$ is shown in Fig. 7, where $\lambda_1=0.1960\ \mu$m. A linear relation holds within the tolerance of the data, and yields $\Delta\mathcal{E}/\mathcal{E}_1=-3.74\times10^{-2}$ and $\Delta\mathcal{F}/\mathcal{F}_1=9.13\times10^{-2}$. The factor K defined by the equation[5]

$$K=-\frac{1}{2}\frac{(\Delta\mathcal{F}/\mathcal{F}_1)}{(\Delta\mathcal{E}/\mathcal{E}_1)} \quad (12)$$

is 1.2, and the sign is opposite to that for several oxides such as $BaTiO_3$, TiO_2, and KTN.[5,22]

Dispersion relations for the temperature coefficients $dn_i/n_i dT$ and $d\rho/\rho\,dT$ can be derived from Eqs. (5) and (8), respectively, for the single-oscillator model.[8] The results are

$$\left(\frac{1}{n_i}\frac{dn_i}{dT}\right)\frac{n_i^2}{n_i^2-1}=-\frac{\lambda^2}{\lambda^2-\lambda_i^2}\,\Delta_i+\tfrac{1}{2}\Omega_i\,, \quad (13)$$

where $\Delta_i=d\mathcal{E}_i/\mathcal{E}_i dT$ and $\Omega_i=d\mathcal{F}_i/\mathcal{F}_i dT$, and

$$\frac{1}{\rho}\frac{d\rho}{dT}=-\frac{\lambda^2}{\lambda^2-\lambda_1'^2}\,4\Delta_1'+\Omega_1'\,, \quad (14)$$

where $\Delta_1'=d\mathcal{E}_1'/\mathcal{E}_1' dT$ and $\Omega_1'=d\mathcal{S}_1/\mathcal{S}_1 dT$.

Figures 8 and 9 show plots of Eq. (13) for $dn_i/n_i dT$ and those of Eq. (14) for $d\rho/\rho\,dT$, respectively, using the values of λ_i and λ_1' given in Table III. Values of the parameters obtained are summarized in Table V. The temperature coefficients for the average oscillator positions Δ_i are in agreement with the coefficient of the band gap, $\sim-10^{-4}/°C$, which is estimated from the data shown in Fig. 1. It is noted that Δ_1 for n_O agrees excellently with Δ_1' for ρ. The parameter Ω_i can be divided into two parts; that is,

$$\Omega_i=dN_i/N_i dT+df_i/f_i dT\,. \quad (15)$$

The first term is directly related to the volume change of the crystal, and we have[8]

$$dN_i/N_i dT=-\sum_r a_r\,, \quad (16)$$

where a_r is the linear thermal-expansion coefficient. Using the data on a_r,[16] we find that the contribution

TABLE V. Temperature coefficients of the oscillator position Δ_i and the oscillator strength factor Ω_i in TeO_2 at 25 °C calculated with the single-oscillator model. Definitions of the symbols appear in Eqs. (13) and (14).

Δ_1: -124×10^{-6}/°C	Ω_1: -250×10^{-6}/°C
Δ_3: -91×10^{-6}/°C	Ω_3: -185×10^{-6}/°C
Δ_1': -132×10^{-6}/°C	Ω_1': -600×10^{-6}/°C

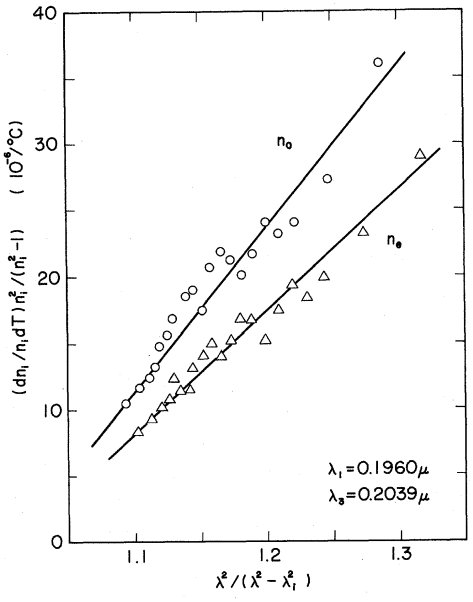

FIG. 8. Dispersion of the temperature coefficients of the refractive indices in TeO_2 at 25 °C. The data shown in Fig. 4 are replotted using Eq. (13) for the single-oscillator model.

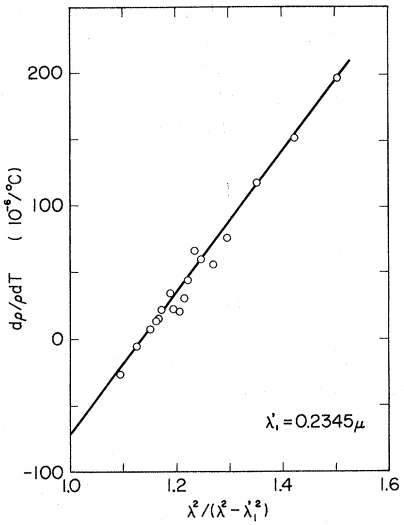

FIG. 9. Dispersion of the temperature coefficient of the optical rotatory power in TeO_2 at 25 °C. The data shown in Fig. 5 are replotted using Eq. (14) for the single-oscillator model.

of the volume change to Ω_i is $-47\times10^{-6}/°C$ and that the main part of Ω_i is thus attributable to changes in the transition probability. The difference $\Omega_1' - \Omega_1$ gives the contribution of changes in the gyration factor g_1, and it is found that this contribution forms the major part of Ω_1'.

The dispersion of the photoelastic constants was discussed by Wemple and DiDomenico[10] using the single-oscillator model. The dispersion relation derived by them can be redefined in our notation as

$$\frac{n_i^4 p_{ij}}{n_i^2-1}=\frac{\lambda^2}{\lambda^2-\lambda_i^2}\,2\delta_{ij}-\omega_{ij}\,, \tag{17}$$

where $\delta_{ij}=d\mathcal{E}_i/\mathcal{E}_i dS_j$ and $\omega_{ij}=d\mathcal{F}_i/\mathcal{F}_i dS_j$. The deformation potential $\mathfrak{D}_{ij}$ defined by them is related to the parameter δ_{ij} by

$$\mathfrak{D}_{ij}=\mathcal{E}_i\delta_{ij}\,, \tag{18}$$

and the factor $\mathcal{K}_{ij}$ is

$$\mathcal{K}_{ij}=-\omega_{ij}/2\delta_{ij}\,. \tag{19}$$

Values of δ_{ij} and ω_{ij} derived from Fig. 6 are summarized in Table VI. It is found that coefficients δ_{13} and δ_{33} with respect to the strain S_3 are negative, while δ_{31} with respect to S_1 is positive. The coefficient δ_{12} related to S_1 is also positive, if we assume that δ_{11} is small considering the extremely small value of p_{11}.[3] Concerning the coefficients ω_{ij}, we find that the magnitudes of ω_{13} and ω_{33} are large, while those of ω_{31} and ω_{12} are small assuming that ω_{11} is not large. The remarkable contrast observed in the magnitudes of ω_{ij} directly corresponds to the anisotropy in p_{ij}: large values of p_{13} and p_{33}, and the relatively small values of p_{31} and p_{12}.

The contribution of the photoelastic effect to the behavior of $dn_i/n_i dT$ can be calculated using the values of δ_{ij} and ω_{ij}. The temperature coefficient of the oscillator position Δ_i and that of the oscillator strength factor Ω_i are given by

$$\Delta_i=\delta_{ij}a_j+\Delta_i^{\,S} \tag{20}$$

and

$$\Omega_i=\omega_{ij}a_j+\Omega_i^{\,S}\,, \tag{21}$$

where a_j is the linear thermal-expansion coefficient, and the superscript S denotes constant strain. The terms $\Delta_i^{\,S}$ and $\Omega_i^{\,S}$ represent an intrinsic thermal effect. Calculated values of $\delta_{3j}a_j$ and $\omega_{3j}a_j$ are as follows:

$$\begin{aligned}\delta_{3j}a_j&=4.0\times10^{-6}/°C\,,\\ \omega_{3j}a_j&=-30\times10^{-6}/°C\,.\end{aligned} \tag{22}$$

Values of $\delta_{1j}a_j$ and $\omega_{1j}a_j$ are nearly equal to $\delta_{3j}a_j$ and $\omega_{3j}a_j$, respectively, assuming that both δ_{11} and ω_{11} are small. It can be seen that the sign of $\delta_{ij}a_j$ is opposite to that of Δ_i. The contribution of the photoelastic effect associated with the thermal expansion is found to be 10–20% to Ω_i, while that to Δ_i is, at most, several percent in magnitude. The temperature coefficient of n_e due to this effect is evaluated as $\sim -17\times10^{-6}/°C$ in the visible spectral region (note that the sign is opposite to the observed one), and we can conclude that the intrinsic part is predominant in the temperature variation of the refractive index. The contribution of the photoelastic effect was calculated in several materials using the published data on $dn_i/n_i dT$, p_{ij}, and a_j.[28] The results show that the observed coefficient $dn_i/n_i dT$ is almost completely attributable to the photoelastic effect in alkali halides, and is mainly due to this effect in MgO and quartz, contrary to the present case.

Finally, the anomalous behavior observed in the dispersion of $dn_i/n_i dT$ and $d\rho/\rho\, dT$ is discussed. Extremely weak absorption, about 0.4% for $E \parallel a$ axis and smaller for $E \parallel c$ axis, was observed in the vicinity of 0.55 μm by measuring the external transmittance of the 1-cm-thick specimen. The

TABLE VI. Values of the oscillator position change δ_{ij} and the oscillator strength change ω_{ij} due to strain in TeO_2 at room temperature. Definitions of δ_{ij} and ω_{ij} appear in Eq. (17).

$\delta_{12}-\delta_{11}$:	0.48	$\omega_{12}-\omega_{11}$:	−0.11
δ_{13}:	−0.80	ω_{13}:	−4.08
δ_{31}:	0.14	ω_{31}:	−0.36
δ_{33}:	−0.25	ω_{33}:	−2.34

absorption seems to split into two peaks located approximately at 0.52 and 0.57 μm, and each absorption peak fits the relation[29]

$$\alpha_i = \frac{(2\pi e/hc)\mathcal{F}_i \mathcal{E}_i \mathcal{E}^2 \gamma_i}{(\mathcal{E}_i^2 - \mathcal{E}^2)^2 + \gamma_i^2 \mathcal{E}_i^2 \mathcal{E}^2} \quad , \tag{23}$$

with $\mathcal{F}_i \sim 1.5\times10^{-8}$ eV^2 and damping factor $\gamma_i \sim 10^{-1}$. Using the following equation for the real part of the refractive index in the absorption region,

$$n_i^2 - 1 = \frac{\mathcal{F}_i(\mathcal{E}_i^2 - \mathcal{E}^2)}{(\mathcal{E}_i^2 - \mathcal{E}^2)^2 + \gamma_i^2 \mathcal{E}_i^2 \mathcal{E}^2} \quad , \tag{24}$$

and its differential form with respect to temperature, these absorption peaks are found to contribute to $n_i^2 - 1$ only in the order of 10^{-8} at $\mathcal{E} = (1 \pm \gamma_i)^{1/2}\mathcal{E}_i$ and do not influence the behavior of $dn_i/n_i dT$ to an observable extent. On the other hand, two small anomalous peaks of ρ, about 0.3°/mm, were observed at 0.52 and 0.57 μm. The rotatory power at the absorption region is represented by

$$\rho = \mathcal{G}_1 \frac{\mathcal{E}^2(\mathcal{E}_1^2 - \mathcal{E}^2)^2 + \gamma_1^2 \mathcal{E}^6}{[(\mathcal{E}_1^2 - \mathcal{E}^2)^2 + \gamma_1^2 \mathcal{E}_1^2 \mathcal{E}^2]^2} \tag{25}$$

instead of Eq. (8), and each anomalous peak leads an extremely large value of the gyration factor $g_1 (\sim 4\times10^3$ rad/mm). If we accept such a large value of g_1, it is possible to explain the anomalous behavior of $d\rho/\rho\, dT$ using the differential form of Eq. (25) with respect to temperature with $\Delta_1 \sim 4\times10^{-4}$/°C and $\Omega_1' \sim -5\times10^{-3}$/°C. These values of Δ_1 and Ω_1' are reasonable comparing the behavior of $d\rho/\rho\, dT$ at 80 °C to that at 25 °C, as shown in Fig. 5. More detailed experiments will be necessary for a satisfactory quantitative explanation of these anomalies.

V. CONCLUSION

Absorption at the fundamental band edge in the ultraviolet region and dispersion characteristics of the refractive indices, the optical rotatory power along the optic axis, associated temperature coefficients, and the photoelastic constants have been investigated in single-crystal TeO_2.

Refractive-index data at 20 °C are discussed using the well-known Sellmeier dispersion relation of single- and two-oscillator descriptions.[5] The single-oscillator relation exhibits a significant deviation from the experimental data below 0.45 μm, while the two-term relation with oscillators located at 9.24 and 4.70 eV excellently fits the data over the entire wavelength region, 0.4 – 1.0 μm. The contribution of the former oscillator to the refractive index is larger than that of the latter. The dispersion energies $\mathcal{E}_{di}$[6] for the transition at 9.24 eV are 23.9 eV for n_0 and 26.1 eV for n_e, and are in agreement with the values obtained for the averaged single oscillator. These trends are also valid for BO_6-type oxides, such as TiO_2, $SrTiO_3$, and $LiNbO_3$.

Optical rotation of this crystal is always left handed in the present specimens. Its dispersion is explained by the two-term Chandrasekhar's formula[7] with oscillator positions nearly equal to those for the refractive indices. Dispersion energy $\mathcal{E}_{d1}'$ is defined on the analogy of that for the refractive index, and the value for the transition at 9.3 eV is in fair agreement with that for the average transition in the single-oscillator model.

The signs of the photoelastic constants, the magnitudes and the relative signs of which are already known,[3] are determined by the present experiment. Dispersion measurements of the photoelastic constants reveal that a large anisotropy exists between the changes of the oscillator strength factor and position induced by S_1 and those induced by S_3.

Dispersion characteristics of $dn_i/n_i dT$ and $d\rho/\rho\, dT$ show that the temperature coefficients of the oscillator position and strength are negative. The main contribution to the positive value of $dn_i/n_i dT$ comes from an intrinsic temperature effect, and the contribution of the photoelastic effect associated with the thermal expansion is negative. Anomalous behavior is observed in the dispersion of $dn_i/n_i dT$ and $d\rho/\rho\, dT$ between 0.5 and 0.6 μm, probably attributable to extremely weak absorption peaks located in this wavelength region.

ACKNOWLEDGMENTS

The author is much indebted to N. Niizeki for helpful discussion and a critical reading of the manuscript, H. Iwasaki and S. Miyazawa for supplying TeO_2 single crystals, T. Kasai for the expert fabrication of the specimen for measurements of the rotatory power and the absorption coefficient, S. Saito for the sample preparation and some parts of the measurements, and Y. Ohmachi for the measurement of the refractive indices in the infrared region.

[1] J. Liebertz, Krist. Technik 4, 221 (1969).
[2] G. Arlt and H. Schweppe, Solid State Commun. 6, 783 (1968).
[3] N. Uchida and Y. Ohmachi, J. Appl. Phys. 40, 4692 (1969).
[4] J. Leciejewicz, Z. Krist. 116, 345 (1961).
[5] M. DiDomenico, Jr. and S. H. Wemple, J. Appl. Phys. 40, 720 (1969).
[6] S. H. Wemple and M. DiDomenico, Jr., Phys. Rev. Letters 23, 1156 (1969).
[7] S. Chandrasekhar, Proc. Indian Acad. Sci. A 37, 468 (1953); Proc. Roy. Soc. (London) 259, 531 (1961).
[8] R. S. Krishnan, *Progress in Crystal Physics* (Central Art Press, Madras, India, 1958), Vol. I, Chap. 5.

[9]See Chap. 4 in Ref. 8.
[10]S. H. Wemple and M. DiDomenico, Jr., Phys. Rev. B 1, 193 (1970).
[11]N. Uchida, S. Miyazawa, and S. Saito, J. Phys. Soc. Japan 28, 800 (1970).
[12]F. Urbach, Phys. Rev. 92, 1324 (1953).
[13]M. DiDomenico, Jr. and S. H. Wemple, Phys. Rev. 166, 565 (1968).
[14]A. Frova, Nuovo Cimento 55B, 1 (1968).
[15]J. F. Nye, *Physical Properties of Crystals* (Oxford U.P., Oxford, England, 1957), p. 261.
[16]Y. Ohmachi and N. Uchida, J. Appl. Phys. 41, 2307 (1970).
[17]See pp. 83 and 254 in Ref. 15.
[18]W. L. Bond, J. Appl. Phys. 36, 1674 (1965).
[19]*American Institute of Physics Handbook* (McGraw-Hill, New York, 1963), Sec. 6, p. 33.
[20]S. B. Levin, N. J. Field, F. M. Plock, and L. Merker, J. Opt. Soc. Am. 45, 737 (1955).
[21]A. A. Giardini, J. Opt. Soc. Am. 47, 726 (1957).
[22]S. H. Wemple, M. DiDomenico, Jr., and I. Camlibel, J. Phys. Chem. Solids 29, 1797 (1968).
[23]N. Uchida, S. Miyazawa, and K. Ninomiya, J. Opt. Soc. Am. 60, 1375 (1970).
[24]The value of δ_d for TeO_2 was already given as 23.2 eV in Table I of Ref. 6, and the present results indicate that this value is for n_o.
[25]H. Iwasaki, H. Toyoda, N. Niizeki, and H. Kubota, Japan. J. Appl. Phys. 6, 1101 (1967).
[26]M. Cardona, Phys. Rev. 140, A651 (1965).
[27]S. K. Kurtz, in *Proceedings of the International Meeting on Ferroelectricity*, edited by V. Dvorak, A. Fouskova, and P. Glogar (Publishing House, Czechoslovak Academy of Science, Prague, 1966), Vol. I, p. 413.
[28]See Chaps. 1, 4, and 5 in Ref. 8; see also Secs. 4 and 6 in Ref. 19.
[29]F. Seitz, *The Modern Theory of Solids* (McGraw-Hill, New York, 1940), p. 634.

PHYSICAL REVIEW B VOLUME 4, NUMBER 10 15 NOVEMBER 1971

Aggregation of Pb^{2+} Impurities in NaCl and KCl†

W. C. Collins* and J. H. Crawford, Jr.
Department of Physics, University of North Carolina, Chapel Hill, North Carolina 27514
(Received 2 August 1971)

The aggregation of Pb^{2+} impurity-vacancy complexes has been studied by measurement of dielectric loss and ionic thermocurrents (ITC) in KCl and NaCl and by the decay of luminescence in NaCl. A third-order reaction has been observed to govern the loss of complexes in crystals with high Pb content (above 100 ppm), while for dilute crystals (under 20 ppm) the reaction order is neither second nor third. The decay of luminescence in dilute NaCl was also neither second nor third order but was faster than the ITC decay.

Precipitation of impurities from solid solution in ionic crystals is a topic of considerable interest and the aggregation of divalent cation impurities in alkali halides has been the subject of extensive investigations in recent years.[1-4] Because of charge compensation by cation vacancies and Coulombic interactions between the compensating defect and the doubly charged impurity ion, nearly all of the dissolved impurity is in the form of dipolar impurity-vacancy complexes at temperatures below ~150 °C. This configuration provides a ready means of impurity transport[5] since both vacancy-impurity interchange and reorientation occur with appreciable rates above room temperature. The rate of the transport process and hence the rate of impurity precipitation from supersaturated solution will be limited by the slowest of these two steps. Since the complexes possess a permanent dipole moment, their rate of loss from solution during the aggregation process can be monitored conveniently via measurements of (a) dielectric loss,[5] (b) transient depolarization current,[6] or (c) ionic thermocurrent (ITC).[7] Moreover, in the case of paramagnetic impurities the progress of the aggregation reaction can be observed by means of electron paramagnetic resonance[8] (EPR) or, in the rare event that the impurity in the complex has an optical transition which is distinct from that in the aggregated form, the exciting or emitted photon can be used as an index of the concentration of impurity-vacancy complexes. It has been established[9,10] that the 315-nm emission band of NaCl: Pb is of this type; the 315-nm emission decreases in intensity as aggregation occurs.

Cook and Dryden[1] first measured the aggregation of divalent impurity-vacancy dipoles in $NaCl:Ca^{2+}$. They observed that the initial decay of dielectric loss was governed by a third-order process, which implies that the first stage of aggregation is the simultaneous union of three dipoles forming a trimer. This was a surprising result since the probability of a random encounter of a pair of dipoles should be much larger than for the simultaneous encounter of three dipoles. Further, rough calculations have shown that the planar quadrupole configuration of two dipoles has only slightly less